




Application of ultrasonic cleaning for shipborne heat exchangers: Construction, numerical simulation, and verification

Hauke Buse¹✉, Lars Spangemacher², Siegmund Fröhlich³

¹  <https://orcid.org/0000-0002-4763-9325>

²  <https://orcid.org/0000-0003-0589-0981>

³  <https://orcid.org/0000-0002-5532-5975>

^{1,2} Thyssenkrupp Marine Systems, Emden

³ Proceconsult.de

✉ corresponding author, e-mail: hauke.buse@thyssenkrupp.com

Keywords: ultrasonic, cleaning, heat exchanger, pipe bundle, micro-cavitation, simulation

JEL Classification: Q53, Q55, L95, L99

Abstract

The current article describes the basics and prospects of the ultrasound-assisted cleaning of shell and tube heat exchangers that are used, e.g., on ships. A main issue of seawater heat exchangers is their clogging. After a certain operating time, the fouling process (barnacles, algae, etc.) starts, which results in a decreased performance that produces a noticeably reduced flow rate and a declining transmission of heat energy. Based on the current state of the art, heat exchangers are cleaned by mechanical or chemical (CIP, cleaning in place) methods. Especially on ship-based systems, a mechanical cleaning in very narrow spaces can be difficult and the usage of chemicals for CIP may generally be prohibited. An ultrasound-assisted cleaning would significantly save time and manning. Based on previous experiments, a test reactor represented by a shell and tube heat exchanger with ultrasound-assisted cleaning has been designed. A FEM (finite element method) simulation is performed to provide information about the ultrasound power distribution inside the reactor. Further, the assembly and commissioning of the test reactor with associated comparative measurements were carried out, which are also reported here.

Introduction

Heat exchangers play an essential role in the operability of ships. They provide cooling for the engine, the air conditioning, or other equipment with substantial heat dissipation onboard. The primary task of a heat exchanger is to transfer thermal energy from one medium (e.g., a fluid, a gaseous medium, or even a mixture of both) to another, spatially separated medium. The transport of the energy occurs as a result of a temperature gradient, whereby the heat is transferred from the higher to the lower energy level. The two most common types of heat exchangers (Figure 1) on board ships are “shell and tube bundle

heat exchangers” and “plate heat exchangers”. The first type was chosen for our tests and simulations.

Shell and tube heat exchangers consist of a number of tubes arranged in certain patterns (e.g., parallel alignment), through which the first medium (water, in this case) flows, while the so-called “mantle space” has a second medium flown through it. Plate heat exchangers, on the other hand, are made of wave-shape profiled plates. These plates are arranged so that a heat-absorbing fluid follows the heat-emitting fluid (VDI, 2013).

Regular cleaning is necessary to ensure the proper operation of the heat exchanger and, thus, all the systems connected to it. The cleaning of shell and

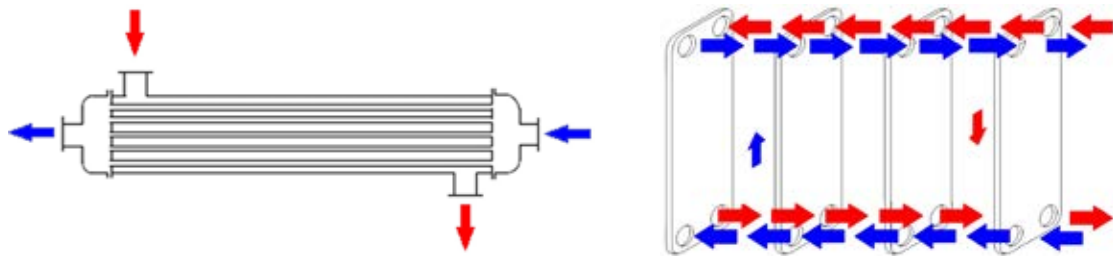


Figure 1. Schematic views of common heat exchangers. Left: shell and tube heat exchanger. Right: plate heat exchanger (according to Baehr & Stephan, 2016 and Miao et al., 2017), in which red represents “hot” fluid and blue is “cold” fluid

tube heat exchangers is associated with costs and downtime, since it has to be dismantled prior to the mechanical cleaning of the shell wall, as well as the pipe bundle. In order to ensure a tightness after the cleaning, the heat exchanger is subject to a pressure test.

Ultrasonic cleaning as an approach for maintenance reduced operation

A (periodically applied) ultrasound-assisted cleaning of the shell and tube heat exchanger is intended to reduce the costs of cleaning manually. Ultrasound (by definition, in the range 20 kHz – 1 GHz) has become one of the most important areas of technical acoustics today. There is a variety of applications, which includes to name just a few: imaging in medical diagnostics, non-destructive material testing, power ultrasound for work pieces and tool cleaning, and soldering or material welding (Grote & Feldhusen, 2014). Beside acoustic streaming (i.e., the movement of water due to acoustic emission) or warming, micro-cavitation is the most important effect when it comes to cleaning applications by means of ultrasonic radiation.

Acoustic cavitation as underlying physical principle of ultrasonic assisted cleaning

Cavitation is the formation and subsequent implosion of vapor bubbles within liquids. Large negative pressure amplitudes cause this phenomenon from propagating sound waves. The cavitation is initiated by gas purges or impurities (cavitation nuclei). During the negative pressure phase of the shaft, the medium can then “tear open” at this point. The resulting cavity is filled with gas or steam that forms a bubble. The periodic oscillation of the sound waves causes the bubbles to grow to a certain size before their implosion (Müller & Möser, 2017).

The cavitation bubble collapse shown in Figure 2 determines the underlying cleaning effect of the

ultrasound. The formation of a jet close to the surface detaches dirt particles that are adhered to the surface to be cleaned. Hence, the cavitation bubbles are larger and vibrate stronger at low excitations, for which the cleaning power is largely determined by the frequency. Typical cleaning frequencies range from 20 kHz (figuratively speaking this is like cleaning with a brush) and 100 kHz upwards (like cleaning with a fine brush) (Lerch, Sessler & Wolf, 2009). Due to the size of the heat exchanger and the grade of fouling, a frequency range of 20 kHz to 40 kHz has been chosen.

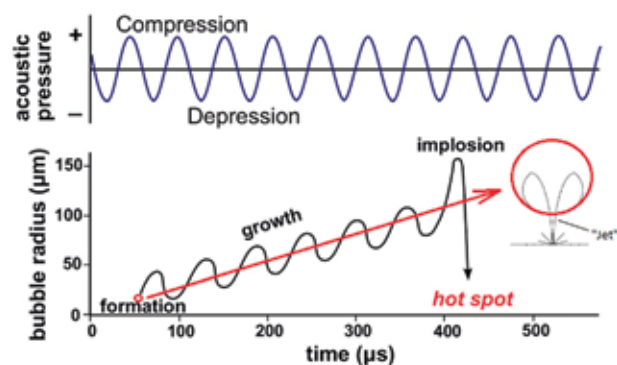


Figure 2. Schematic illustration of the process of acoustic cavitation: the formation, growth, and implosive collapse of bubbles, which generate cavitation jets (adapted from Xu, Zeiger & Suslick, 2013)

Construction of the test reactor and simulation of US power distribution

In order to study the ultrasonic cleaning effects on a shell and tube heat exchanger, initial experiments were carried out on a test reactor (Figure 3) (here, the medium is tap water, volume is 55 l, diameter is 320 mm, and material is 1.4571).

The ultrasonic radiation is transmitted into the reactor from 3 planes that are circularly arranged at an angle of 120° by means of so-called pusher-rods (or transmission elements) (Figure 4). These rods transfer the vibrations that originates from the

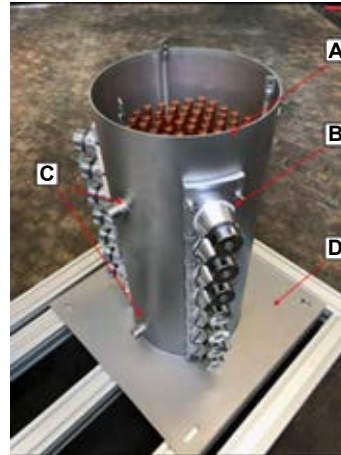
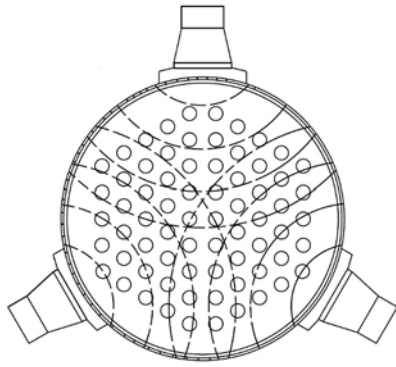


Figure 3. Left: principle of ultrasonic assisted cleaning and location of the ultrasonic transducers. Right: assembled reactor, in which A – pipes representing tube bundle, B – pusher-rod with transducers, C – inlet/outlet for flow through applications, and D – base plate

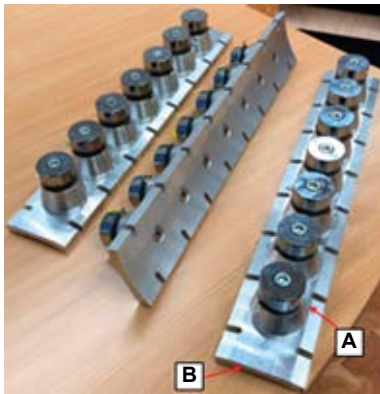


Figure 4. Assembled pusher-rods. Here, A – ultrasonic transducer (120 W @ 28 kHz; C = 7800 pF) and B – aluminum pusher-rod carrying seven transducers in parallel alignment

transducers flat radiating area (“head”) to the curved surface of the reactor wall and from this position into the water. The resonating frequency of the assembled rods has been mechanically tuned (by adding the mass of the rod to the head mass of the transducers) to ~26 kHz. While many parameters such as the area and thickness of the radiating surface, number of transducers (including their tail- and head-masses), and the piezo ceramics define the conclusive resonating frequency, the calculation based on this is far more complex. Thus, the authors refer the reader to (Chen, 2011) for a detailed description of the topic.

Simulation described

A FEM simulation was carried out before the construction of the reactor, which was used to study

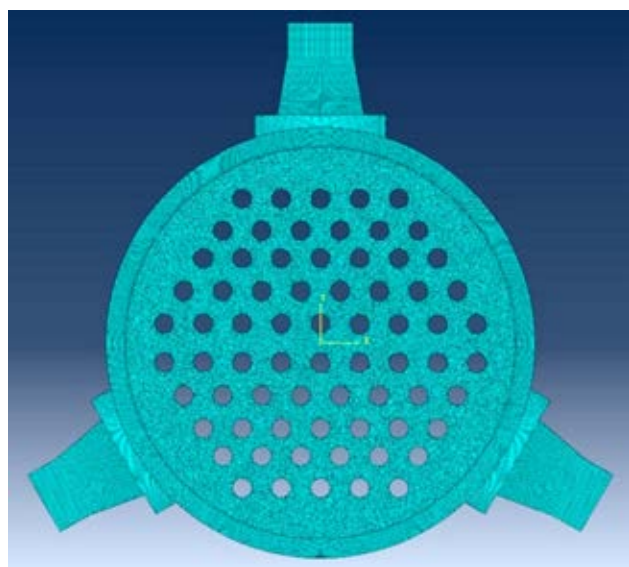
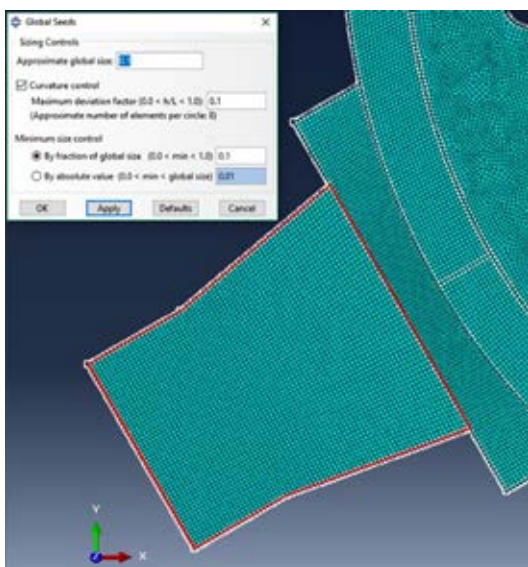


Figure 5. Meshing chosen for the simulation of the pressure distribution. Left: detailed view of the meshing across a transducer, which is attached to the reactor by means of a pusher-rod. Right: global view across the reactor surface

the distribution of the ultrasonic power within the volume. From this, initial conclusions can be drawn that identify the cleanup or poor-cleaning zones, due to any interferences. Interference describes the change in amplitude for the superposition of two or more waves. If the waves cancel each other out, we speak of a destructive interference; in contrast, constructive interference describes the amplification of wavefronts. For the FEM simulation, the software Abaqus/Simulia was utilized in a 1:10 ratio model of the test reactor. This scale-down was necessary in order to reduce the complexity of the computation.

A meshing based on the hexahedral finite elements (C3D8R) with a length of 0.1 mm – shown in Figure 5 – has been chosen. Assuming an excitation frequency of 28 kHz results in a “wavelength to mesh” ratio of $\lambda = v/f = 1600 \text{ m/s [water]} / 28000 \text{ Hz} = 57 \text{ mm}$ (for 1:10 model ratio $\cong 1:57$ lambda to mesh ratio), which overachieves the recommendation by at least 10 samples over the full-width half-maximum (FWHM) (Palmeri et al., 2017).

FEM simulation results

Two sets of simulations had been carried out: a) distribution of the acoustic power within the water filled reactor without a pipe bundle and b) distribution of the acoustic power within the water filled reactor with an inserted pipe bundle.

Figures 6 and 7 show the wave propagation within one period ($T = 3.6 \times 10^{-5} \text{ s}$, $\cong 28 \text{ kHz}$). The pressure shift is represented by the color spectrum, starting from blue (no shift) to red (strong shift). After $1.4 \times 10^{-5} \text{ s}$, one can observe constructive interference of the sound waves at the outer edges (middle figures). For Figure 7, at $2.2 \times 10^{-5} \text{ s}$, the simulation is showing more even wave propagation throughout the reactor, which includes the pipe bundle (lower left corner), compared to the “empty” reactor. In addition, Figure 8 shows a 3-dimensional visualization of the pressure distribution having been calculated, which shows the propagation within the entire volume of the reactor (with inserted pipes).

A temperature risen by approximately 2.45 K, within 17.5 min, has been observed during the reproducible measurements (70 points at 15 s sampling time). With a specific thermal capacity, C_{Water} , of 4.187 kJ/kg K and a volume of approximately 40 l, this relates to a transferred energy of 0.381 kW/h. Considering a driving electrical current of $\sim 4.4 \text{ A}$, rated at 300 V, this corresponds to 1/3 of the input power that is transformed, measurable, and acts as a heater. However, such a warming effect can be neglected due to the non-constant application of the ultrasonic-assisted cleaning.

Figure 9 once again shows that constructive interference develops, especially at the outer edges between the pusher-rods.

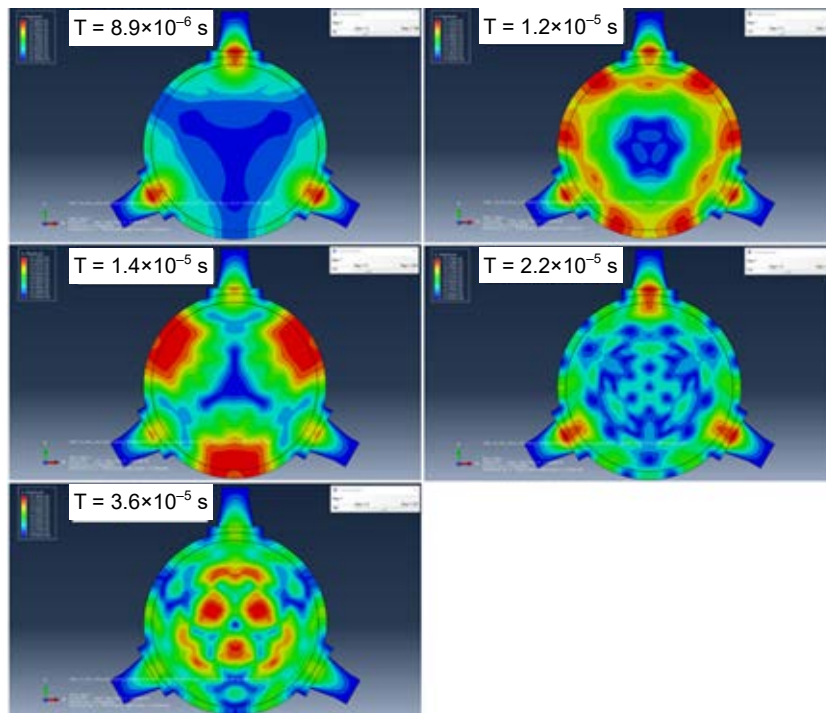


Figure 6. Time slices showing the propagation of the acoustic wavefronts, which emerge from the transducers through the reactor volume, without any inserted pipes

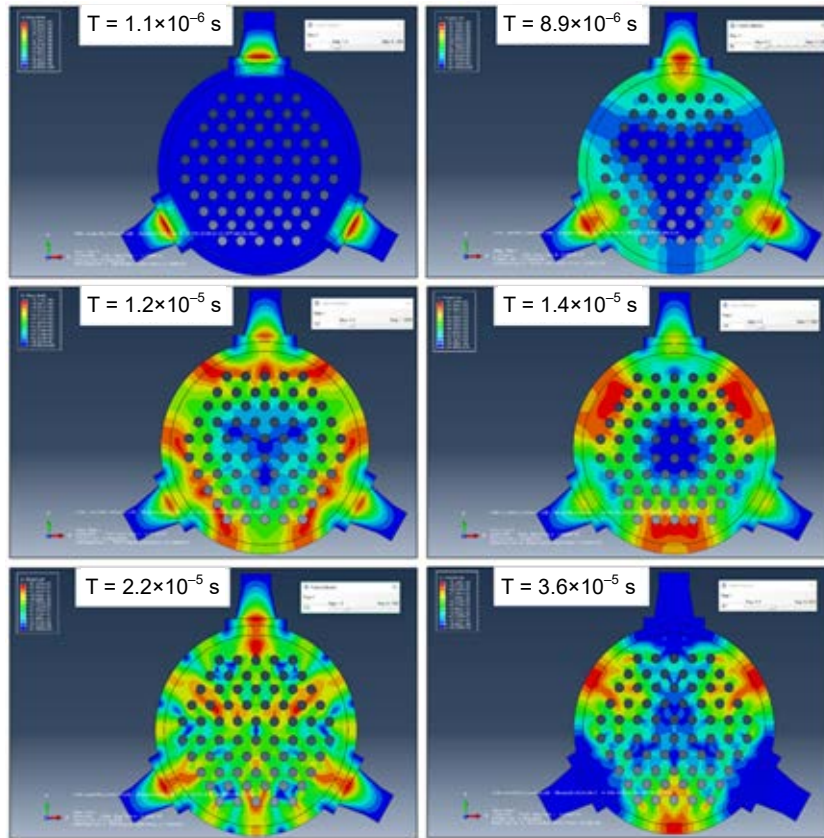


Figure 7. As Figure 6, but with inserted pipes

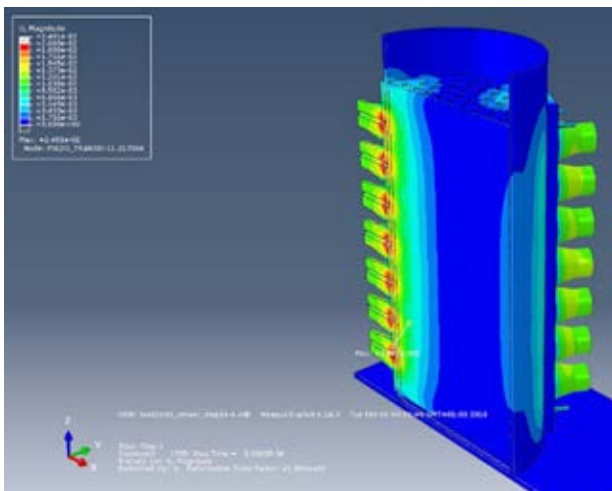


Figure 8. 3-dimensional visualization of the acoustic wave propagation after 8×10^{-6} s

Set-up and metrological verification

After the successful simulation of the 3-dimensional power distribution, which shows the regions of constructive and destructive interference, the set-up and metrological verification of the reactor can be carried out (Figure 10).

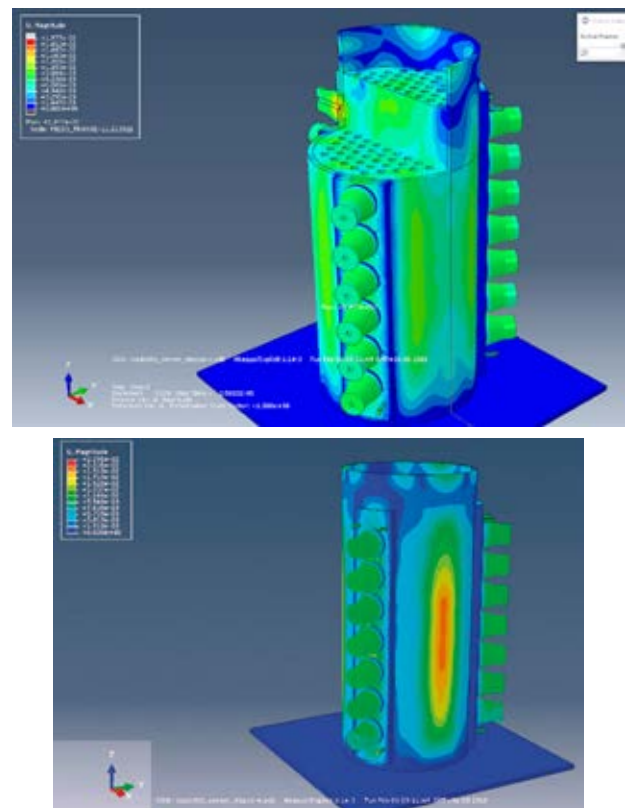


Figure 9. Top: 3D visualization showing an even sound wave distribution through the reactor volume. Bottom: 3D visualization of the construction at the outer shell between the pusher-rods

The strength of the ultrasonic radiation represents the acoustic pressure that has been measured inside the reactor by means of an ultrasonic probe within one plane. This probe was constructed from a piezo disc that is attached to a metal stem, which converts

the deflection of the stem into a corresponding voltage. In the first test run, 70 measurements were performed in a pointwise manner in one plane, which accords to the tube grid arrangement but without the tube bundle installed (Figure 11).

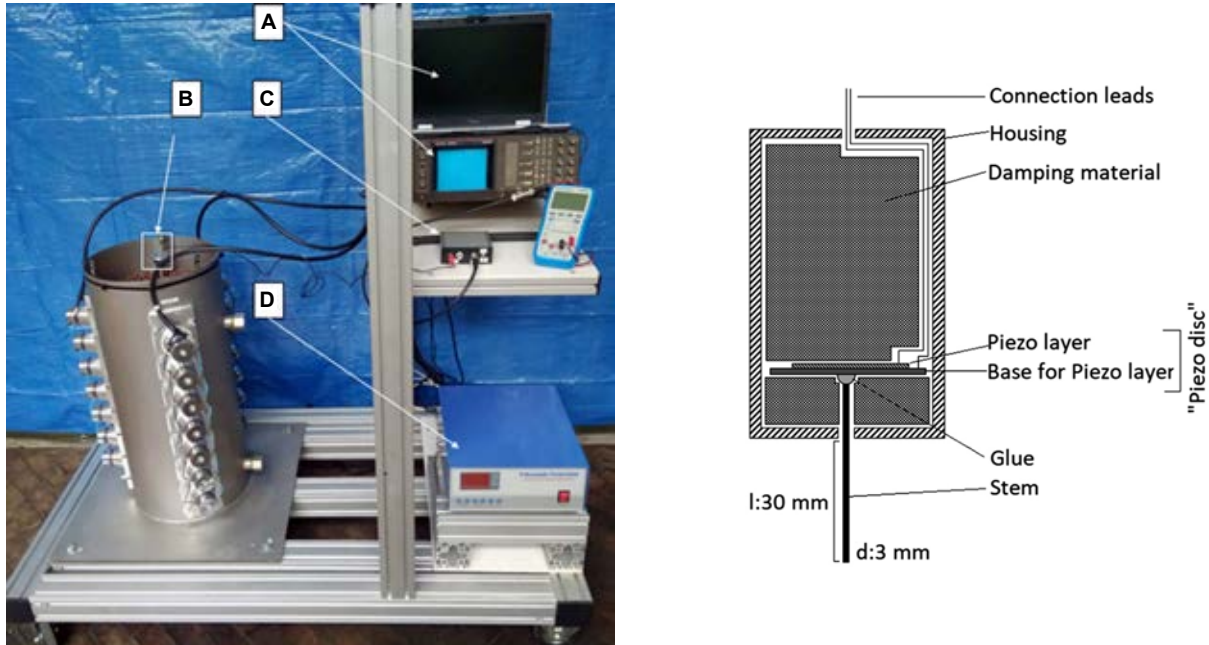


Figure 10. Left: test rig for the ultrasonic test reactor, in which A – data acquisition, B – piezo measuring probe (own development), C – measuring amplifier for the piezo measuring device (own development), and D – ultrasound generator (commercial grade). Right: schematic view of the ultrasonic test probe for the acoustic pressure measurement

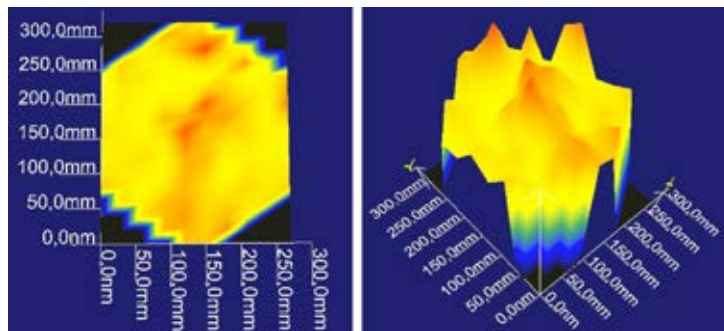


Figure 11. Measurements without the tube bundle. Left: acoustic power in plain view. Right: same data in 3-dimensional view (arbitrary units shown as red to blue, representing the highest to the lowest measured amplitude of the acoustic power)

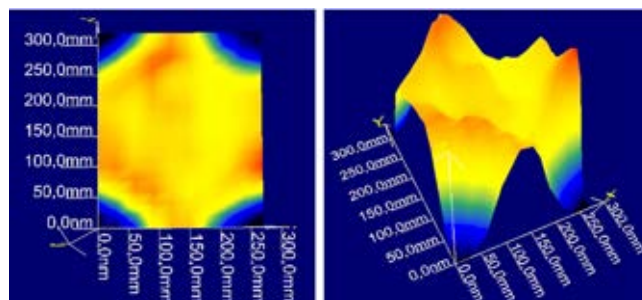


Figure 12. Measurement with the tube bundle. Left: acoustic power in plain view. Right: same data in 3-dimensional view (color coding as Figure 11)

In the second experimental series, the tube bundle was installed into the reactor and measurements were carried out in each individual copper tube, again this resulted in 70 measuring points (Figure 12).

Conclusion and outlook

An ultrasonic test reactor, representing a shell and tube heat exchanger, has been constructed and successfully put into operation. The FEM simulation of the acoustic pressure distribution and the experimental measurements are consistent, which represent the sound propagation and the associated interference areas. These are important findings since they are particularly useful for further project investigations. Furthermore, the efficiency of the reactor can be enhanced, e.g., by reducing the thickness of the pusher-rod, while accepting the need for an adjustment of the resonance frequency.

By adaptation of the piezo probe (e.g., a lengthening of the stem), subsequent measurements within the multiple planes of the reactor volume can be carried out. Moreover, the application of three ultrasonic generators could enhance the power fed to the pusher-rods, and the sweep frequency would additionally allow a phase independence between the rods. This can result in changing areas of constructive interference, which minimize possible material damage due to the prevention of static cavitation peaks. Additionally, long-term experiments

with real marine media are expected to be executed soon, to demonstrate the functionality of the descaling of barnacles, mussels, algae, and other intruders that prevents heat exchanger clogging for long-time operations.

References

1. BAEHR, H.D. & STEPHAN, K. (2016) *Wärme- und Stoffübertragung*. 9. Auflage. Berlin Heidelberg: Springer-Verlag.
2. CHEN, Y.-C. (2011) A comparative assessment of classification methods for resonance frequency prediction of Langevin piezoelectric transducers. *Applied Mathematical Modelling* 35, 7, pp. 3334–3344.
3. GROTE, K.H. & FELDHUSEN, J. (2014) *Dubbel Taschenbuch für Maschinenbau*. 24. Auflage. Berlin Heidelberg: Springer-Verlag.
4. LERCH, R., SESSLER, G. & WOLF, D. (2009) *Technische Akustik*. 1. Auflage. Berlin Heidelberg: Springer-Verlag.
5. MIAO, Q., YOU, S., ZHENG, W., ZHENG, X., ZHANG, H. & WANG, Y. (2017) A grey-box dynamic model of plate heat exchangers used in an urban heating system. *Energies* 10, p. 1398.
6. MÜLLER, G. & Möser, M. (2017) *Ultraschall in Medizin und Technik*. Berlin Heidelberg: Springer-Verlag.
7. PALMERI, M., QIANG, B., CHEN, S. & URBAN, M. (2017) Guidelines for finite-element modeling of acoustic radiation force-induced shear wave propagation in tissue-mimicking media. *IEEE Transactions on Ultrasonics, Ferroelectrics, and Frequency Control* 64, 1, pp. 78–92.
8. VDI (2013) *VDI-Wärmeatlas*. 11. Auflage. Berlin Heidelberg: Springer-Verlag.
9. XU, H., ZEIGER, B.W. & SUSLICK, K.S. (2013) Sonochemical synthesis of nanomaterials. *Chemical Society Reviews* 42, 7, pp. 2555–2567.

Cite as: Buse, H., Spangemacher, L., Fröhlich, S. (2022) Application of ultrasonic cleaning for shipborne heat exchangers: Construction, numerical simulation, and verification. *Scientific Journals of the Maritime University of Szczecin, Zeszyty Naukowe Akademii Morskiej w Szczecinie* 71 (143), 41–47.